# Dendritic $Ca^{2+}$ dynamics and multi-modal processing in a cricket antennal interneuron

**Timothy George Bayley[1] and Berthold Hedwig[1]**

Corresponding author: bh202@cam.ac.uk

Running title – Multi-modal processing in a cricket interneuron

[1] Department of Zoology, University of Cambridge, Cambridge, Cambridgeshire, CB2 3EJ, UK.

**Abstract**

The integration of stimuli of different modalities is fundamental to information processing within the nervous system. A descending interneuron in the cricket brain, with prominent dendrites in the deutocerebrum, receives input from three sensory modalities: touch of the antennal flagellum, strain of the antennal base, and visual stimulation. Using calcium imaging, we demonstrate that each modality drives a $Ca^{2+}$ increase in a different dendritic region. Moreover, touch of the flagellum is represented in a topographic map along the neuron's dendrites. Using intracellular recording, we investigated the effects of $Ca^{2+}$ on spike shape through the application of the $Ca^{2+}$ channel antagonist, $Cd^{2+}$, and identified probable $Ca^{2+}$-dependent $K^+$ currents.

**New & Noteworthy**

Different dendritic regions of the cricket brain neuron DBNi1-2 showed localised $Ca^{2+}$ increases when three modalities of stimulation (touch of the flagellum, strain at antennal base and visual input) were given. Touch stimulation induces localised $Ca^{2+}$ increases according to a topographic map of the antenna. $Ca^{2+}$ appears to activate $K^+$ currents in DBNi1-2.

**Keywords**

Multi-modal stimulation, Dendritic processing, $Ca^{2+}$ imaging.

## Introduction

Multi-modal processing is essential to adjust the output of the nervous system given a range of sensory inputs. In the cricket brain, a giant interneuron, DBNi1-2 (descending brain neuron ipsilateral 1-2), responds to three modalities of input – touch to the flagellum (the elongate region comprising the majority of the antenna), strain of the antennal base, and visual stimulation (Staudacher and Schildberger, 2000; Gebhardt and Honegger, 2001; Schöneich et al., 2011). Here, we investigate how the location of its synaptic inputs, and morphology of its dendrites, contributes to multi-modal processing.

The overlap between DBNi1-2 dendrites and projections of neurons carrying sensory information differs for each modality. Hair-like touch receptors, trichoid sensilla (Pumphrey, 1936; Pflüger, 1980), are located along the flagellum, (Fudalewicz-Niemczyk and Rościszewska, 1973; Staudacher et al., 2005; Watanabe et al., 2012). Their axonal terminals overlap with large "finger-like" dendrites of DBNi1-2 (Gebhardt and Honegger, 2001; Staudacher and Schildberger, 2000). Strain receptors, campaniform sensilla (Pringle, 1938a, 1938b; Spinola and Chapman, 1975), are found at the base of the antenna (Fudalewicz-Niemczyk and Rościszewska, 1973; Staudacher et al., 2005). Their terminals overlap with a different region, the junction between the finger-like dendrites and the axon descending to the thoracic segments (Schöneich, 2008). Visual input to DBNi1-2 comes via the optic stalk (Gebhardt and Honegger, 2001), and projections from it overlap with a more-anterior dendritic region (Honegger and Schürmann, 1975; Gebhardt and Honegger, 2001; Schöneich et al., 2011). These morphological features imply that the sensory input of each modality is received in a separate dendritic region of DBNi1-2. Sensory responses of the neuron may be reduced during active antennal movements (Gebhardt and Honegger, 2001), but this is not addressed here.

The spatial arrangement of synaptic inputs to a neuron can be revealed using *in-vivo* optical imaging techniques. Here, we focused on $Ca^{2+}$ imaging, because it has been studied extensively, and indicators are reliable. Considerable progress has been made through single cell calcium imaging of

large neurons in insects, where the entire range of sensory afferents of a particular modality forms connections with a single neuron, such as for mechanosensory (Ogawa et al., 2004), auditory (Baden and Hedwig, 2007; Presern et al., 2015), and visual interneurons (Borst and Egelhaaf, 1992; Peron et al., 2009; Hopp et al., 2014). The location of synaptic inputs to single neurons has also been studied in mammals, including amacrine cells in the retina (Euler et al., 2002; Grimes et al., 2010), and various brain neurons, such as pyramidal neurons in the cortex (Jia et al., 2010) and hippocampus (Sheffield and Dombeck, 2014). However, in vertebrates each neuron often only receives a subset of the afferent input of a sensory field.

Although the role of DBNi1-2 in behaviour is not yet known, the spatial separation of sensory inputs has important functional implications for how multiple inputs are processed within a single neuron (reviews: Koch and Segev, 2000; London and Häusser, 2005). We have investigated whether different dendritic regions of DBNi1-2 show a $Ca^{2+}$ increase in response to touch and strain of the antenna, and visual stimulation. By combining calcium imaging with intracellular recordings, we first assess the restriction of $Ca^{2+}$ signals to specific dendritic regions. Second, we explore the role of $Ca^{2+}$ on neuronal processing through the application of the calcium channel blocker, $Cd^{2+}$.

## Materials & Methods

### *Animals*

Adult male and female crickets (*Gryllus bimaculatus*) were taken from a stock in the Department of Zoology. Crickets were kept on a 12:12 h light:dark cycle and fed ad libitum with cat food, fish flakes, muesli, and water.

### *Dissection*

The head was secured in a modified Eppendorf tube after removing the mouthparts (Fig. 1B). The tube was filled with saline of ionic concentrations (in mM): NaCl – 135, KCl – 10, $CaCl_2$ – 7, $NaHCO_3$ – 8, $MgCl_2$ – 1, TES – 4.8, trehalose – 4.4. The brain was then exposed, with the descending connectives left intact, but with antennal motor nerves N2, N3 and N4 (Honegger et al., 1990) cut. The brain was supported on a stainless steel platform, attached to a metal tube through which a light guide was passed to illuminate the recording site.

### *Electrophysiology*

For intracellular recording, borosilicate glass capillaries (OD 1.0 mm and ID 0.7 mm, Hilgenberg, Malsfeld, Germany) were pulled using a DMZ Universal Puller (Zeitz Instruments, Martinsried, Germany) to form electrodes of 50-70 MΩ resistance when filled. For imaging, two dyes were introduced to the microcapillaries by back-filling: a calcium indicator, 0.5 mM Oregon Green 488 BAPTA-1 (OGB-1, Molecular Probes, Life Technologies Ltd. Paisley, UK); and a fixable dye which allowed the morphology of the neuron to be inspected after imaging, 0.15 mM Alexa Fluor®-568 (Alexa-568, Molecular Probes). Dyes were dissolved in UltraPure™ water (Invitrogen, Life Technologies Ltd. Paisley, UK) to ensure a low $Ca^{2+}$ concentration. The shaft was filled with 1 M KAc. The brain was

viewed using a DM-LFS microscope (Leica Microsystems, Wetzlar, Germany) equipped with 4x and 10x air objectives, and 10x and 20x water-immersion objectives. The focal neuron, DBNi1-2, was located visually from landmarks on the surface of the brain, with the electrode inserted at the junction between the antennal lobe and ventral area of flagellar afferents (Staudacher and Schildberger, 2000). It was further characterised electrophysiologically from its large background level of EPSPs, as well as its response to light and antennal touch, which is very uncommon for neurons within this region of the brain (Gebhardt and Honegger, 2001; Schöneich et al., 2011). The electrode signal was amplified with an SEC-10x amplifier (npi electronic, Tamm, Germany) and fed into a Powerlab 8/30 data acquisition system (AD Instruments, Oxford, UK), recorded at 50 kHz in Labchart software (AD Instruments). For morphological analysis, the brain was dissected, fixed in 5 % paraformaldehyde, dehydrated for 30 mins each in a series of 70, 90, 95 and 100 % ethanol, and cleared in methyl salicylate. After clearing, images were taken either with an EOS 350D DSLR camera (Canon UK Ltd., Reigate, UK) mounted on an Axiophot microscope (Carl Zeiss Microscopy Ltd., Cambridge, UK), or with a TCS-SP-5 confocal microscope (Leica), using LAS AF software.

*Optical imaging*

An Optoscan monochromator (Cairn Research Ltd., Kent, UK) provided a uniform epifluorescent illumination of the preparation with light of 488 ± 15 nm to excite OGB-1, or 568 ± 15 nm to excite Alexa-568. Light emitted by the indicator was captured by an iXon DV887DCS-BV cooled CCD camera (Andor Technology Ltd., Belfast, UK), mounted onto the microscope. 128x128 pixel images were acquired at 50 Hz, with 20 ms exposure time, using Andor iQ software. For synchronisation with electrophysiological data, the camera provided pulses when capturing each frame, which were recorded simultaneously with electrophysiological data. Fluorescence signals are expressed as the relative percentage change in fluorescence from background, $\Delta F/F$ (%).

To quantify the position of $Ca^{2+}$ increase in the neuron, the mid-points of the fluorescence profiles in the antero-posterior and medio-lateral axes were derived. These are based on calculations for the centre of mass of an object (e.g. Fig. 2Ai). For a rectangular ROI, the mean $\Delta F/F$ along the medio-lateral (M-L) axis was calculated by averaging the values of all corresponding pixels in the antero-posterior (A-P) axis: all A-P data were collapsed on the M-L axis, e.g. pixel ($M\text{-}L_1/A\text{-}P_1$) average of pixel ($M\text{-}L_1/A\text{-}P_1$) to pixel ($M\text{-}L_1/A\text{-}P_n$) etc. The mean $\Delta F/F$ along the antero-posterior axis was calculated correspondingly by averaging the values of all pixels in the medio-lateral axis: all M-L data were collapsed on the A-P axis, e.g. pixel ($M\text{-}L_1/A\text{-}P_1$) average of pixel ($M\text{-}L_1/A\text{-}P_1$) to pixel ($M\text{-}L_n/A\text{-}P_1$). These values were smoothed with a 10-pixel moving average, before selecting the pixels > 75 % of the maximum $\Delta F/F$ intensity, and normalising all pixels to a value of 0-1. For pixels above 75% the distance of each pixel from the posterior-most, or lateral-most, position was multiplied by its normalised intensity, and divided by the sum of the normalised intensity of all the pixels above 75% intensity. This provided the mid-point of fluorescence in the antero-posterior and medio-lateral axis, respectively. Anterior and posterior were defined according the neuraxis of insect nervous systems (Ito et al. 2014).

*Stimulation*

Based on morphological data, the descending antennal interneuron, DBNi1-2, is thought to receive inputs in distinct dendritic regions from sensory neurons responding either to touch of the antennal flagellum (blue region in Fig. 1A; Gebhardt and Honegger, 2001; Staudacher and Schildberger, 2000), strain at the base of the antenna (magenta region in Fig. 1A; Schöneich, 2008) or visual stimulation of the compound eyes (yellow region in Fig. 1A; Honegger and Schürmann, 1975; Gebhardt and Honegger, 2001; Schöneich et al., 2011). For touch-sensitive trichoid sensilla (Staudacher and Schildberger, 2000) and strain-sensitive campaniform sensilla (Schöneich, 2008), simultaneous labelling of the sensory fibres and DBNi1-2 revealed a close spatial association between the afferent

axons and the dendrites of DBNi1-2. For visual input, stainings were not obtained in the same animals (Honegger and Schürmann, 1975; Gebhardt and Honegger, 2001).

To activate touch-sensitive mechanoreceptors on the flagellum, electrical stimulation was used, as mechanical stimulation of the flagellum also activates the campaniform sensilla at the antennal base (Schöneich, 2008). The afferent fibres are thought to project in the flagellar nerve such that mechanoreceptors at the tip of the flagellum run through the centre of the nerve and those further towards the base run more laterally (Fudalewicz-Niemczyk and Rościszewska, 1972). To ensure only the mechanoreceptors at the focal site were activated, small stimulus intensities were used to excite only more lateral afferents in the nerve. Up to three small incisions were made in the flagellar cuticle, into which two 20 µm steel-wires (Rheinische Feindraht Industrie, Eckenhagen, Germany) were inserted, insulated up to their tips. The area was coated with petroleum jelly to prevent desiccation. Stimulation was with a 1 ms pulse of 1 V amplitude, which would drive one or two spikes in DBNi1-2. Further details are given later in the text.

To excite strain-sensitive campaniform sensilla at the base of the antenna, 2.5 mN tactile stimuli were presented with an insect pin glued to a small speaker cone. The base of the antenna is also endowed with several other receptor neuron types, including the sensilla of the scapal hair plate, and a chordotonal organ, as well as trichoid and basiconic sensilla (Fudalewicz-Niemczyk and Rościszewska, 1973; Rospars, 1988). The receptor neurons from the scapal hair plate and chordotonal organ pass through a separate nerve branch, different from the other receptor types (Gebhardt and Honegger, 2001). Previous experiments have shown that stimulating this branch does not induce a response in DBNi1-2, suggesting that there is no synaptic input from these sensory neurons (Gebhardt and Honegger, 2001). The chemosensory sensilla terminate in a separate neuropile, which does not overlap with the dendrites of DBNi1-2 (Staudacher and Schildberger, 2000). Therefore inputs to DBNi1-2 should primarily arise from the trichoid sensilla, projecting to the finger-like dendrites, and campaniform sensilla, projecting to the junction region of these dendrites (Schöneich, 2008).

Visual stimuli were presented using a white LED placed 15 cm from the right eye of the cricket. Light pulses were of 10 ms duration, and were driven by scripts written in Spike2 (CED, Cambridge, UK). Exact stimulus parameters are provided in the text. The stimuli may have activated both the compound eyes and ocelli, however, input to DBNi1-2 is likely to come only from the eyes: firstly, when the optic stalks are ablated, the visual input to DBNi1-2 is abolished (Gebhardt and Honegger, 2001); and secondly, the dendrites of DBNi1-2 overlap with the neurons projecting from the optic stalk (Honegger and Schürmann, 1975) and not with those from the ocelli (Koontz, 1976). Epifluorescent illumination also stimulated the visual system, but spiking subsided within 1 s.

*Blockade of $Ca^{2+}$ channels*

To block $Ca^{2+}$ channels, saline containing 0.1 M $CdCl_2$ was continually passed over the preparation, excess saline was removed with a Masterflex L/S pump (Cole-Palmer Instrument Co., London, UK).

*Data analysis*

Data were processed in Spike2 (CED, Cambridge, UK) and Excel (Microsoft Corporation, Redmond, WA, USA), with statistical tests carried out in R (R Foundation, Vienna, Austria). Images were analysed in ImageJ, Spike2, and Python 2.7 (Python Software Foundation, DE, USA). Data were tested for normality with a Shapiro-Wilk test. Values in the text are given in mean ± standard error unless otherwise stated.

## Results

To identify whether the different sensory modalities activate different dendritic regions of DBNi1-2, a calcium indicator, Oregon Green BAPTA-1 (OGB-1), was introduced through a glass microelectrode, and each modality was presented independently (Fig. 1A,B). DBNi1-2 was imaged in the brain using epifluorescence microscopy. This technique allows large sections of the neuron to be imaged simultaneously, including a **f**inger-like **r**egion of dendritic arborisation ('**fr**' in Fig. 1C), the **j**unction **r**egion of these dendrites ('**jr**' in Fig. 1C), and a separate **a**nterior **r**egion ('**ar**' in Fig. 1C), representing a section of the projection to the putative site of visual input. The more anterior dendritic regions are located dorsally, deep within the brain and due to the resulting light scatter could not be imaged clearly. The accessible regions, however, were imaged at high spatial and temporal resolution. The site of $Ca^{2+}$ increase was calibrated between animals by aligning to the posterior-most and lateral-most position of the neuron (Fig. 1C).

### *Modality-specific localisation of $Ca^{2+}$*

A modality-specific localisation of $Ca^{2+}$ signals should only occur if: 1) synaptic inputs are spatially separated based on modality; 2) a $Ca^{2+}$ increase occurs at a dendrite when it receives synaptic inputs; and 3) any such $Ca^{2+}$ increase is restricted to a specific region of the dendrites. Spiking activity may drive $Ca^{2+}$ increases, which would be expected to be highest in the spike-generating zone (Peron and Gabbiani, 2009). In DBNi1-2, this is likely to be where the dendritic regions converge (Gwilliam and Burrows, 1980) and where the descending axon originates (arrowhead in Fig. 1C). If $Ca^{2+}$ influx is derived from spikes, it would be expected to occur in this same position for all modalities of input.

To quantify the location of $Ca^{2+}$ increases in the DBNi1-2 dendrites during sensory stimulation, the fluorescence profile was measured from the start of stimulation for 400 ms (or 20 frames) for the medio-lateral, and antero-posterior axes (profiles shown above and right Fig. 2Ai-iii, respectively, see

Methods). A threshold was taken at 75 % (grey region in profiles), and the weighted mid-point of the pixels above the threshold was then calculated (indicated by black and grey lines in Fig. 2Ai-iii, see Materials & Methods). The range and mean position of the mid-point was calculated between animals. Data are from four animals responding to all three stimuli, with a further four analysed for their response to trichoid sensilla.

When electrically stimulating touch-sensitive trichoid sensilla, in the example shown, the fluorescence midpoint occurred 61 µm medially from the lateral-most point of the neuron, and 113 µm anteriorly from the posterior-most point (Fig. 2Ai; Movie 1). Across all the preparations, stimulated at various points along the flagellum, it fell between 37 and 112 µm medially, and between 16 and 158 µm anteriorly, with a mean position of 87 ± 7 µm medially, and 104 ± 13 µm anteriorly (Fig. 2Bi; N = 8). In all animals, therefore, the fluorescence mid-points fell within the area of the finger-like dendrites, onto which flagellar mechanoreceptors are thought to form synapses (Staudacher and Schildberger, 2000).

When strain-sensitive campaniform sensilla at the antennal base were activated in this animal, the fluorescence mid-point was different; occurring 143 µm medially, and 74 µm anteriorly (Fig. 2Aii; Movie 1). Between preparations, it occurred from 124 to 143 µm medially, and 51 to 86 µm anteriorly, with a mean position of 129 ± 3 µm medially and 74 ± 8 µm anteriorly (Fig. 2Aii, Bii, N = 4). These points are all around the junction region of the finger-like dendrites (note that two data points completely overlap), where campaniform sensilla from the base of the antenna have been indicated to form synapses with DBNi1-2 (Schöneich, 2008).

Stimulating the visual system with light pulses (Fig. 2Aiii; Movie 1), drove a fluorescence increase with its mid-point 168 µm medially and 105 µm anteriorly. Between preparations the position of the strongest response ranged from 133 and 176 µm medially and 68 and 112 µm anteriorly, with a mean position of 151 ± 9 µm medially and 88 ± 11 µm anteriorly (Fig. 2Biii, N = 4). These points fall within the junction region of the finger-like dendrites and the neurite projecting to the anterior

dendrite which is indicated to overlap with visual neurons (Honegger and Schürmann, 1975; Gebhardt and Honegger, 2001; Schöneich et al., 2011).

When the fluorescence images for all three stimulus modalities were overlaid, the spatial distribution of the responses showed little overlap (Fig. 2Aiv; cyan represents touch; magenta, strain; and yellow, visual stimulation). Similarly, when the mid-points to all modalities of stimulation were overlaid (Fig. 2Biv), the regions activated by flagellar stimulation were distinct from the regions activated by other stimuli. Only the regions active upon antennal base stimulation and visual stimulation showed an overlap. This overlap is likely to be accentuated by scatter of the fluorescent light in the tissue, which will reduce and broaden the signal from the deep anterior dendrites receiving visual inputs. Spike-derived $Ca^{2+}$ influx may also contribute to blurring the spatial separation of the $Ca^{2+}$ signals. However, despite this overlap, there was a clear difference in the regions showing a $Ca^{2+}$ increase for each modality of stimulation, suggesting that the synaptic inputs to the dendrites of DBNi1-2 are separated according to modality, and that this is reflected in localised increases in intracellular $Ca^{2+}$ as demonstrated in Fig. 2Aiv and schematically represented in Fig. 2C. This also suggests that local synaptic inputs are driving the $Ca^{2+}$ increase, and not spikes, which would be expected to drive a more widespread $Ca^{2+}$ increase.

*Time-course of $Ca^{2+}$ signals*

To assess the amplitude and time-course of $Ca^{2+}$ signals in different dendritic areas, separate regions of interest (ROIs) were used to select the dendritic regions ‘fr’, ‘jr’ and ‘ar’ (Fig. 2Di). To quantify the relative increase in $Ca^{2+}$ to each modality of stimulation, the change in fluorescence from baseline ($\Delta F/F$) was measured in each ROI (Fig. 2Dii-iv, Ei) and normalised to the maximum fluorescence in all ROIs to each modality of stimulation (Fig. 2Eii). In all ROIs, the greatest $\Delta F/F$ occurred in response to flagellar stimulation (blue in Fig. 2Dii-iv, Ei), however scatter may have influenced this effect, as well

as spike-derived $Ca^{2+}$ signals. Without normalisation, the response to touch receptor stimulation was 7.9 ± 2.8 %, and occurred in region 'fr' (blue in Fig. 2Eii). Antennal base stimulation induced the highest $\Delta F/F$, 2.3 ± 0.1 %, in region 'jr' (magenta in Fig. 2Dii-iv, Fig. 2 Ei, ii). Visual stimulation induced the largest $\Delta F/F$, 2.2 ± 0.5 %, in region 'ar' (yellow in Fig. 2Dii-iv and Fig. 2Ei, ii). Measured in the ROI with the highest $\Delta F/F$, the decay of the $Ca^{2+}$ response was similar for each stimulus modality, with a time constant of 1.1 ± 0.4 s for flagellar stimulation, 1.2 ± 0.4 s for antennal base stimulation, and 1.4 ± 0.4 s for visual stimulation ($\tau_d$ to 37%, p = 0.54, ANOVA, N = 4).

*Localisation of $Ca^{2+}$ signals upon flagellar stimulation*

As the mid-point of fluorescence differed between animals with their flagellum stimulated at various points (Fig. 2Bi), the correlation between the position of antennal stimulation and the localisation of the fluorescence increase in the finger-like region of the dendrites was explored. The total length of the flagellum varied from 20-28 mm between animals (mean 25 ± 2 mm, N = 10 males and 10 females). Up to three extracellular stimulating electrodes were inserted into the flagellum at points between 2 and 28 mm from the base (Fig. 3A). Only the finger-like dendrites of DBNi1-2 were imaged during these experiments (Fig. 3B).

The fluorescence profile in DBNi1-2 is presented for a single animal with three stimulating electrodes inserted into its flagellum (Fig. 3C). Stimulation at 8 mm from the base of the scape elicited the highest $\Delta F/F$ in a posterior region of the finger-like dendrites, with the mid-point 109 µm medially from the lateral-most point and 40 µm anteriorly from the posterior-most point of these dendrites (Fig. 3Ci, Movie 2). Stimulation at the middle of the flagellum (19 mm from the base) elicited the highest $\Delta F/F$ in a region more lateral and anterior, with the mid-point 37 µm medially and 121 µm anteriorly (Fig. 3Cii). Stimulation close to the tip, (28 mm from the base) induced the highest $\Delta F/F$ in a more medial and anterior region, with its mid-point 112 µm medially and 142 µm anteriorly (Fig.

297 3Ciii). When overlaid, these regions of highest $\Delta F/F$ were clearly separated (Fig. 3D). In addition, when
298 ROIs were used to select an anterior, middle, and posterior region of the finger-like dendrites (Fig.
299 3Bii), an independent fluorescence increase occurred in each ROI for the different positions of flagellar
300 stimulation, with very little cross-talk (Fig. 3E). The amplitude of the $Ca^{2+}$ increase differed between
301 each region.

302 When averaged between 11 stimulation positions in 5 animals, a positive correlation was
303 found between the position of the stimulating electrodes along the flagellum and the position of the
304 mid-point of fluorescence (Fig. 3Fi): the anterior distance of the mid-point scaled linearly with a slope
305 of 4.8 μm from the posterior tip of the dendritic arborisation per mm distance along the flagellum (Fig.
306 3Fii; $R^2 = 0.64$, $p = 0.003$, $N = 5$). Together, these data suggest that a topographic map of touch to the
307 flagellum exists in this antennal neuropile region, with the proximal-to-distal axis of the flagellum
308 represented along the posterior-to-anterior axis of the neuropil and the DBNi1-2 finger-like dendrites
309 (summarised in Fig. 3G).

310 The topography of inputs from the visual system and the campaniform sensilla was not
311 investigated. The campaniform sensilla come in a small cluster at the base of the antenna (Fudalewicz-
312 Niemczyk and Rościszewska, 1973; Staudacher et al., 2005) and only form synapses with a restricted
313 area of DBNi1-2 (Schöneich, 2008).

314

315 *Relationship between $Ca^{2+}$ signals and spiking*

316 As calcium indicators were introduced with intracellular microelectrodes, for the same stimuli the
317 spiking response of DBNi1-2 could be compared with the fluorescence signals. The electrode was
318 usually inserted into one of the large branches of the finger-like dendrites (black circle in Fig. 4, bottom
319 centre). Stimulating touch-sensitive receptors in the middle of the flagellum (14 ± 1.8 mm) elicited 2.2
320 ± 0.6 spikes (Fig. 4Aii, N = 4). The latency to the first spike varied, from 6.4 to 38.5 ms, depending upon

the distance of the stimulation site from the antennal base (Fig. 4Aii, inset; N = 7). Stimulation of strain receptors at the antennal base elicited 2.5 ± 0.5 spikes at a latency of 5.5 ± 0.4 ms (Fig. 4B, D; N = 7), and visual stimulation elicited 1.4 ± 0.3 spikes, at a much longer latency of 53 ± 1.8 ms (Fig. 4C, D; N = 7). In each case, a rapid $Ca^{2+}$ increase occurred concurrently with the onset of spiking, increasing to its maximum intensity within 40 ms, or 2 frames of imaging (Fig. 4Ai-Ci). The decay in fluorescence was much slower and took over 1 s, as noted previously.

In three ROIs ('fr',' jr', and 'ar', Fig. 4, bottom centre), the relative $\Delta F/F$ was compared within each animal with the number of spikes to each stimulus (Fig. 4E). The $\Delta F/F$ occurring with a spike was different for each modality of stimulation: for example, in area 'fr', flagellar stimulation induced the highest increase, 4.4 ± 2.0 % ΔF/F per spike, whereas in area 'jr', strain to the antennal base induced 0.6 ± 0.1 % ΔF/F per spike, and in area 'ar', visual stimulation induced 1.6 ± 0.8 % ΔF/F per spike (Fig. 4E). The latter value is likely to underestimate $\Delta F/F$ to visual stimulation, as the anterior dendrites receiving visual input are located deep in the brain. The range of $\Delta F/F$ coupled with single spikes provides further indication that the fluorescence signal in the dendrites was not derived from spike activity.

*Effect of $Ca^{2+}$ on multi-modal processing*

To test the effects of $Ca^{2+}$ within DBNi1-2, $Cd^{2+}$, a $Ca^{2+}$ channel blocker, was bath-applied to the preparation. Bath application should not affect spike generation in afferent neurons, as they are located peripherally, in the antennae or optic stalk.

Intracellular recordings of spikes of DBNi1-2 were compared before and after application of $Cd^{2+}$. Individual spikes occurring with a large inter-spike interval and generated without direct sensory simulation, were used to avoid analysing compound responses. The duration of the $K^{+}$-dependent repolarisation phase of each action potential increased gradually over time (Fig. 5A-B). 20 min after

345 application of $Cd^{2+}$, overall a mean significant increase in the time constant $\tau$ of the repolarisation
346 phase occurred, from 1.3 ± 0.4 to 2.1 ± 0.7 ms (Fig. 5B, p = 0.04, paired t-test, N = 3). This change in
347 action potential shape indicates that a reduction or absence of $Ca^{2+}$ in the neuron results in fewer $K^+$
348 channels being open, suggesting that $Ca^{2+}$-sensitive $K^+$ currents are present (Savić et al., 2001;
349 Sivaramakrishnan and Oliver, 2001). When combined with the discovery of localised $Ca^{2+}$ currents in
350 DBNi1-2, this provides a possibility that $Ca^{2+}$ is directly involved in multi-modal processing through
351 localised changes in $K^+$ ion conductivity.

352

353 **Discussion**

354 We have investigated how the dendritic structure of a cricket antennal neuron, DBNi1-2, relates to
355 the processing of three modalities of sensory input: touch, strain, and visual stimulation. Spatially-
356 restricted increases in $Ca^{2+}$ suggest that the sites of synaptic input to the neuron are different for each
357 modality (Fig. 2; Movie 1). $Ca^{2+}$ signals were further divided for the inputs from touch receptors along
358 the flagellum, which appear to be arranged in a topographic map (Fig. 3; Movie 2). Localised $Ca^{2+}$
359 increases in DBNi1-2 may induce $Ca^{2+}$-sensitive $K^+$ currents (Fig. 4), as tested by applying $Cd^{2+}$ to the
360 preparation (Fig. 5).

361

362 *Separation of synaptic inputs*

363 For all sensory modalities tested, the localised $Ca^{2+}$ increases recorded (Fig. 2) indicate a close
364 correspondence between the morphological projection sites of the relevant sensory neurons
365 described in previous studies (see Introduction) and the location of synaptic input onto the dendrites
366 of DBNi1-2.

367 Electrical stimulation to the flagellum drove a $Ca^{2+}$ increase in the finger-like dendrites of
368 DBNi1-2, in agreement with their morphological overlap with mechanosensory flagellar afferent fibres
369 (Staudacher and Schildberger, 2000). By stimulating the afferent fibres at different lengths along the
370 flagellum, we revealed a topographic map of flagellar afferent projection, with basal afferents
371 projecting posteriorly onto DBNi1-2, and distal afferents projecting anteriorly (Fig. 3; Movie 2).
372 Topographically-arranged $Ca^{2+}$ signals have previously been observed in the auditory neurons of
373 crickets (Baden and Hedwig, 2007), and bush-crickets (Presern et al., 2015), as well as in other insect
374 neurons which receive inputs from maps of different sensory modalities, including neurons that
375 respond to wind stimulation of the cerci of crickets (Ogawa et al., 2004) and to visual stimulation of
376 the eyes of flies (Borst and Egelhaaf, 1992; Spalthoff et al., 2010) and locusts (Peron et al., 2009).

When the antennal base was stimulated mechanically, the region of highest fluorescence increase was at the junction region of the finger-like dendrites of DBNi1-2 (Fig. 2Aii, iv) where the campaniform sensilla synapse onto the neuron (Schöneich, 2008). However, a small fluorescence increase was also observed in a posterior region of the finger-like projections (Fig. 2Aii, iv). This is likely to be due to simultaneous activation of the trichoid sensilla on the basal flagellum, which project to the posterior dendrites, according to the topographic arrangement (Fig. 3).

Frontal visual input to the compound eyes led to a mid-point of fluorescence increase in DBNi1-2 which was specific to an anteriorly-located dendrite (Fig. 2Aiii, Biii, D-E), suggesting that the neuron receives visual input within this region. Although this anterior dendrite was located too deep within the brain to be imaged optimally with our system, no other dendritic region responded to the visual stimulus. A two-photon microscope would allow deeper imaging with a higher spatial resolution (Helmchen and Denk, 2005).

In insects, stimulus-specific local $Ca^{2+}$ signals have also been observed in the locust LGMD (Peron and Gabbiani, 2009; Peron et al., 2009), cercal giant interneurons in the cricket (Ogawa et al., 2004, 2008), and auditory neurons in the cricket (Sobel and Tank, 1994; Baden and Hedwig, 2007) and bush-cricket (Triblehorn and Schul, 2013; Presern et al., 2015). Previous work investigated responses to a single stimulus modality, whereas here we studied the response to multiple modalities within a single neuron.

*$Ca^{2+}$ localisation based on stimulus type*

The localisation of $Ca^{2+}$ signals to specific dendritic regions implies that down-stream effects of $Ca^{2+}$ should also occur locally. The influence of $Ca^{2+}$ on spike shape in DBNi1-2 was tested with $Cd^{2+}$, which is known to block voltage-sensitive $Ca^{2+}$ channels (Huang et al., 1989, Pearson et al., 1993, Tang et al., 2014), and to reduce $Ca^{2+}$ influx upon activation of nicotinic acetylcholine receptors (Thany et

al., 2008). The mechanosensory input to DBNi1-2 is likely cholinergic, similar to locust antennal afferents (Knipper et al., 1989). Therefore, $Cd^{2+}$ should block any $Ca^{2+}$ influx from their activation. Besides this, $Cd^{2+}$ may have a wide range of effects in neurons. For example, in pre-synaptic terminals, $Cd^{2+}$ reduces $Ca^{2+}$ influx (Heidelberger and Matthews, 1992, Mintz et al., 1995) and synaptic efficacy (Mintz et al., 1995). Twenty minutes after application of $Cd^{2}$, the $K^{+}$-dependent repolarisation stage of action potentials was elongated (Fig. 5A-B). This indicates that $Ca^{2+}$ in DBNi1-2 affects $K^{+}$ currents, which are reduced when $Ca^{2+}$ is reduced or absent after addition of $Cd^{2+}$. In future work, this could be corroborated, such as with the use of BAPTA (Triblehorn and Schul, 2013; Presern et al., 2015). The basis for this effect could also be studied focussing on: $Ca^{2+}$-sensitive $K^{+}$ channels; cAMP signalling; or channel phosphorylation (Wicher et al., 2001). The use of pharmacological agents specific to particular classes of $Ca^{2+}$ channels should shed further light on the role of $Ca^{2+}$ in the neuron. However, many agents effective in vertebrates, such as apamin, are not effective in insects (Wicher et al., 2001), making the identification of these channels currently more difficult.

The separation of sensory inputs has important functional implications for multi-modal processing (reviews: Koch and Segev, 2000; London and Häusser, 2005). For example, the passive electrotonic spread of synaptic potentials in one dendritic region may have little effect in distant regions (Grimes et al., 2010; Jacobs et al., 1986; Liu, 2004; Polsky et al., 2004). Dynamic properties may also contribute to localised synaptic processing, such as activity-dependent adaptation (Sanchez-Vives et al., 2000; Savić et al., 2001; Triblehorn and Schul, 2013), or long-term weakening or strengthening of synapses (review: Larkum and Nevian, 2008). Assessing the extent to which these occur within DBNi1-2 would be an interesting avenue for future research.

The localisation of ion channels also has important functional implications: if $Ca^{2+}$-sensitive $K^{+}$ currents occur in the dendrites, their activation could lead to a reduction in response to a subset of inputs (Kurtz et al., 2000; Presern et al., 2015); however if present close to the spike-generating zone, it could lead to a reduction in the response to all stimuli (Benda and Herz, 2003; Peron and Gabbiani,

2009). Higher resolution optical imaging of single dendrites could provide more details of the localisation of $Ca^{2+}$ currents.

*Role of DBNi1-2 in behaviour*

The functional role of DBNi1-2 in behaviour is not yet known. Its projections to the thoracic ganglia are mapped (Schöneich et al., 2011), and a similar neuron, DBNi2-1, has been implicated in turning behaviour when depolarised (Zorović and Hedwig, 2013). DBNi1-2 also shows morphological similarities to a giant neuron in the cockroach (Comer and Baba, 2011), which has also been implicated in turning (Ye and Comer, 1996). Multi-modal processing could therefore be important to influence the decision to turn.

*Relevance to other systems*

This work was undertaken on an insect neuron, which provides two major advantages: firstly, it is easily accessible for intracellular recordings; secondly, it overlaps with large areas of a sensory neuropile, allowing the nature of synaptic inputs to each of its dendritic regions to be functionally mapped. These fundamental properties of DBNi1-2 are comparable to those of neurons in the mammalian nervous system. In a wide range of neurons, functionally different inputs synapse onto different dendritic regions, the location of which can be estimated using calcium imaging (amacrine cells: Euler et al., 2002; Grimes et al., 2010; cortical pyramidal neurons: Hill et al., 2013; hippocampal pyramidal neurons: Sheffield and Dombeck, 2014; cerebellar Purkinje cells: Kitamura and Häusser, 2011). The compartmentalisation of $Ca^{2+}$ signalling allows for local computation through a range of down-stream effects (reviews: London and Häusser, 2005; Branco and Häusser, 2010), and demonstrates the complexity of the processing in single neurons.

449

## Author Contributions

T.G.B. and B.H. conceived and designed the experiments. T.G.B performed the experiments, performed all analysis and wrote the paper. B.H. provided supervisory feedback throughout.


## Acknowledgements

We thank Malcolm Burrows, Pedro Jacob and Caroline Fabre for critical reading of the manuscript. Work was supported by a PhD grant from MRC UK to T.G.B.

458 **References**


459 Bacon JP, Murphey RK. Receptive fields of cricket giant interneurones are related to their dendritic
460 structure. *J. Physiol.* 352, 601–623, 1984.

461 Baden T, Hedwig B. Neurite-specific $Ca^{2+}$ dynamics underlying sound processing in an auditory
462 interneurone. *Dev. Neurobiol.* 67, 68–80, 2007.

463 Benda J, Herz AVM. A universal model for spike-frequency adaptation. *Neural. Comput.* 15, 2523–
464 2564, 2003.

465 Borst A, Egelhaaf M. In vivo imaging of calcium accumulation in fly interneurons as elicited by visual
466 motion stimulation. *Proc. Natl. Acad. Sci. USA*. 89, 4139–4143, 1992.

467 Branco T, Häusser M. The single dendritic branch as a fundamental functional unit in the nervous
468 system. *Curr. Opin. Neurobiol.* 20, 494–502, 2010.

469 Comer C, Baba Y. Active touch in orthopteroid insects: behaviours, multisensory substrates and
470 evolution. *Phil. Trans. R. Soc. Lond. B. Biol. Sci.* 366, 3006–3015, 2011.

471 Euler T, Detwiler PB, Denk W. Directionally selective calcium signals in dendrites of starburst amacrine
472 cells. *Nature.* 418, 845–852, 2002.

473 Fudalewicz-Niemczyk W, Rościszewska M. The peripheric nervous system of the larva of *Gryllus*
474 *domesticus* L. (Orthoptera). Part I. *Antenna. Acta. Biol. Craconviensia.* 16, 209–217, 1973.

475 Gebhardt M, Honegger HW. Physiological characterisation of antennal mechanosensory descending
476 interneurons in an insect (*Gryllus bimaculatus, Gryllus campestris*) brain. *J. Exp. Biol.* 204, 2265–2275,
477 2001.

478 Grimes WN, Zhang J, Graydon CW, Kachar B, Diamond JS. Retinal parallel processors: More than 100
479 independent microcircuits operate within a single interneuron. *Neuron.* 65, 873–885, 2010.

480 Gwilliam BYGF, Burrows M. Electrical characteristics of the membrane of an identified insect motor

481 neurone. *J. Exp. Biol.* 86, 49–61, 1980.

482 Heidelberger R, Matthews G. Calcium influx and calcium current in single synaptic terminals of
483 goldfish retinal bipolar neurons. *J. Physiol.* 447, 235–256, 1992.

484 Helmchen F, Denk W. Deep tissue two-photon microscopy. *Nat. Methods.* 2, 932–940, 2005.

485 Hill DN, Varga Z, Jia H, Sakmann B, Konnerth A. Multibranch activity in basal and tuft dendrites during
486 firing of layer 5 cortical neurons in vivo. *Proc. Natl. Acad. Sci. USA.* 110, 13618–13623, 2013.

487 Honegger HW, Allgäuer C, Klepsch U, Welker J. Morphology of antennal motoneurons in the brains of
488 two crickets, *Gryllus bimaculatus* and *Gryllus campestris*. *J. Comp. Neurol.* 291, 256–268, 1990.

489 Honegger HW, Schürmann FW. Cobalt sulphide staining of optic fibres in the brain of the cricket,
490 *Gryllus campestris*. *Cell. Tissue. Res.* 159, 213–225, 1975.

491 Hopp E, Borst A, Haag J. Subcellular mapping of dendritic activity in optic flow processing neurons. *J.*
492 *Comp. Physiol. A.* 200, 359–370, 2014.

493 Ito K, Shinomiya K, Ito M, Armstrong JD, Boyan G, Hartenstein V, Harzsch S, Heisenberg M, Homberg
494 U, Jenett A, Keshishian H, Restifo LL, Rössler W, Simpson JH, Strausfeld NJ, Strauss R, Vosshall LB,
495 Insect Brain Name Working Group. A Systematic Nomenclature for the Insect Brain. *Neuron* 81,
496 755–765, 2014.

497 Jacobs GA, Miller JP, Murphey RK. Integrative mechanisms controlling directional sensitivity of an
498 identified sensory interneuron. *J. Neurosci.* 6, 2298–2311, 1986.

499 Jia H, Rochefort NL, Chen X, Konnerth A. Dendritic organization of sensory input to cortical neurons in
500 vivo. *Neuroforum.* 16, 236–237, 2010.

501 Kitamura K, Häusser M. Dendritic calcium signaling triggered by spontaneous and sensory-evoked
502 climbing fiber input to cerebellar Purkinje cells in vivo. *J. Neurosci.* 31, 10847–10858, 2011.

503 Knipper M, Strotmann J, Mädler U, Kahle C, Breer H. Monoclonal antibodies against the high affinity
504 choline transport system. *Neurochem. Int.* 14, 217–222, 1989.

505 Koch C, Segev I. The role of single neurons in information processing. *Nat. Neurosci.* 3 Suppl, 1171–
506 1177, 2000.

507 Koontz M. Neuronal pathways from the dorsal ocelli of the house cricket, *Acheta domesticus*. *J.*
508 *Morphol.* 149, 105–120, 1976.

509 Kurtz R, Dürr V, Egelhaaf M. Dendritic calcium accumulation associated with direction-selective
510 adaptation in visual motion-sensitive neurons in vivo. *J. Neurophysiol.* 84, 1914–1923, 2000.

511 Larkum ME, Nevian T. Synaptic clustering by dendritic signalling mechanisms. *Curr. Opin. Neurobiol.*
512 18, 321–331, 2008.

513 Liu G. Local structural balance and functional interaction of excitatory and inhibitory synapses in
514 hippocampal dendrites. *Nat. Neurosci.* 7, 373–379, 2004.

515 London M, Häusser M. Dendritic computation. *Annu. Rev. Neurosci.* 28, 503–532, 2005.

516 Looger LL, Griesbeck O. Genetically encoded neural activity indicators. *Curr. Opin. Neurobiol.* 22, 18–
517 23, 2012.

518 Mintz IM, Sabatini BL, Regehr WG. Calcium control of transmitter release at a cerebellar synapse.
519 *Neuron*. 15, 675–688, 1995.

520 Mutoh H, Mishina Y, Gallero-Salas Y, Knöpfel T. Comparative performance of a genetically-encoded
521 voltage indicator and a blue voltage sensitive dye for large scale cortical voltage imaging. *Front. Cell.*
522 *Neurosci.* 9, 1–8, 2015.

523 Ogawa H, Baba Y, Oka K. Directional sensitivity of dendritic calcium responses to wind stimuli in the
524 cricket giant interneuron. *Neurosci. Lett.* 358, 185–188, 2004.

525 Ogawa H, Cummins GI, Jacobs GA, Oka K. Dendritic design implements algorithm for synaptic
526 extraction of sensory information. *J. Neurosci.* 28, 4592–46032 2008.

527 Peron S, Gabbiani F. Spike frequency adaptation mediates looming stimulus selectivity in a collision-
528 detecting neuron. *Nat. Neurosci.* 12, 318–326, 2009.

529 Peron SP, Jones PW, Gabbiani F. Precise subcellular input retinotopy and its computational
530 consequences in an identified visual interneuron. *Neuron.* 63, 830–842, 2009.

531 Pflüger H-J. The function of hair sensilla on the locust's leg: the role of tibial hairs. *J. Exp. Biol.* 87,
532 163–176, 1980.

533 Polsky A, Mel BW, Schiller J. Computational subunits in thin dendrites of pyramidal cells. *Nat. Neurosci.*
534 7, 621–627, 2004.

535 Presern J, Triblehorn JD, Schul J. Dynamic dendritic compartmentalization underlies stimulus specific
536 adaptation in an insect neuron. *J. Neurophysiol.* 113, 3787-3797, 2015.

537 Pringle JWS. Proprioception in insects I. A new type of mechanical receptor from the palps of the
538 cockroach. *J. Exp. Biol.* 15, 101–113, 1938a.

539 Pringle JWS. Proprioception in insects II. The action of the campaniform sensilla on the legs. *J. Exp.*
540 *Biol.* 15, 114–131, 1938b.

541 Pumphrey RJ. Slow adaptation of a tactile receptor in the leg of the common cockroach. *J. Physiol.*
542 87, 6–7, 1936.

543 Rospars JP. Structure and development of the insect antennodeutocerebral system. *Int. J. Insect*
544 *Morphol. Embryol.* 17, 243–294, 1988.

545 Sanchez-Vives MV, Nowak LG, McCormick DA. Cellular mechanisms of long-lasting adaptation in visual
546 cortical neurons in vitro. *J. Neurosci.* 20, 4286–4299, 2000.

547 Savić N, Pedarzani P, Sciancalepore M. Medium afterhyperpolarization and firing pattern modulation
548 in interneurons of stratum radiatum in the CA3 hippocampal region. *J. Neurophysiol.* 85, 1986–1997,
549 2001.

550 Schöneich S. Charakterisierung und Identifizierung der plurisegmental deszendierenden Interneurone
551 mit antennal-taktilen Eingängen im ZNS der Grille. PhD thesis, University of Leipzig, 2008.

552 Schöneich S, Schildberger K, Stevenson PA. Neuronal organization of a fast-mediating cephalothoracic
553 pathway for antennal-tactile information in the cricket (*Gryllus bimaculatus* De Geer). *J. Comp. Neurol.*
554 519, 1677–1690, 2011.

555 Sheffield MEJ, Dombeck DA. Calcium transient prevalence across the dendritic arbour predicts place
556 field properties. *Nature.* 517, 200–204, 2014.

557 Sivaramakrishnan S, Oliver DL. Distinct K currents result in physiologically distinct cell types in the
558 inferior colliculus of the rat. *J. Neurosci.* 21, 2861–2877, 2001.

559 Sobel E, Tank D. In vivo $Ca^{2+}$ dynamics in a cricket auditory neuron: an example of chemical
560 computation. *Sci. Pap.* 263, 823–826, 1994.

561 Spalthoff C, Egelhaaf M, Tinnefeld P, Kurtz R. Localized direction selective responses in the dendrites
562 of visual interneurons of the fly. BMC Biol 8: 36, 2010

563 Spinola S, Chapman K. Proprioceptive indentation of the campaniform sensilla of cockroach legs. *J.*
564 *Comp. Physiol. A.* 272, 257–272, 1975.

565 Staudacher EM, Gebhardt M, Dürr V. Antennal movements and mechanoreception: neurobiology of
566 active tactile sensors. *Adv. Insect Phys.* 32, 49–205, 2005.

567 Staudacher E, Schildberger K. A newly described neuropile in the deutocerebrum of the cricket:
568 antennal afferents and descending interneurons. *Zoology.* 102, 212-226, 2000.

569 Tang L, Gamal El-Din TM, Payandeh J, Martinez GQ, Heard TM, Scheuer T, Zheng N, Catterall WA.
570 Structural basis for $Ca^{2+}$ selectivity of a voltage-gated calcium channel. *Nature.* 505, 56–61, 2014.

571 Thany SH, Courjaret R, Lapied B. Effect of calcium on nicotine-induced current expressed by an
572 atypical α-bungarotoxin-insensitive nAChR2. *Neurosci. Lett.* 438, 317–321, 2008.

573 Triblehorn JD, Schul J. Dendritic mechanisms contribute to stimulus-specific adaptation in an insect
574 neuron. *J. Neurophysiol.* 110, 2217–2226, 2013.

575 Watanabe H, Haupt SS, Nishino H, Nishikawa M, Yokohari F. Sensillum-specific, topographic
576 projection patterns of olfactory receptor neurons in the antennal lobe of the cockroach *Periplaneta*
577 *americana*. *J. Comp. Neurol.* 520, 1687–1701, 2012.

578 Wicher D, Walther C, Wicher C. Non-synaptic ion channels in insects - basic properties of currents
579 and their modulation in neurons and skeletal muscles. *Prog. Neurobiol.* 64, 431–525, 2001.

580 Ye S, Comer CM. Correspondence of escape-turning behavior with activity of descending
581 mechanosensory interneurons in the cockroach, *Periplaneta americana. J. Neurosci.* 16, 5844–5853,
582 1996.

583 Yoritsune A, Aonuma H. The anatomical pathways for antennal sensory information in the central
584 nervous system of the cricket, *Gryllus bimaculatus. Invert. Neurosci.* 12, 103–117, 2012.

585 Zorović M, Hedwig B. Descending brain neurons in the cricket *Gryllus bimaculatus* (De Geer): auditory
586 responses and impact on walking. *J. Comp. Physiol. A.* 199, 25–34, 2013.

587

588 **Figure Legends**

589

590 **Figure 1 -** Neuronal morphology and experimental overview. A) Outline of half of the brain with the
591 optic nerve (ON) and the antennal nerve (AN). The morphology of DBNi1-2 as reconstructed from an
592 Alexa-568 staining, the soma (so) and descending axon (ax) are indicated. Areas shaded in colour
593 show putative dendritic regions receiving input from touch-sensitive trichoid sensilla (cyan), strain-
594 sensitive campaniform sensilla (magenta), and visual neurons (yellow). B) Experimental setup showing
595 holder for the head made from a modified Eppendorf tube, as well as stimulation methods: electrical
596 stimulation of touch receptors, mechanical stimulation of strain-sensitive receptors with a pin at the
597 base of the antenna; and visual stimulation with a white LED. C) Average of 50 frames of fluorescence
598 signal during *in vivo* imaging with an outline of the brain (dashed grey line) and the antennal nerve
599 (AN). Shaded regions indicate the finger-like dendritic region (fr), the junction region of these
600 projections (jr), and a separate anterior dendritic region (ar). Inset brain diagram (top right) shows
601 region imaged (grey square). Axes indicate calibration between animals. They indicate the distance
602 from the posterior-most position (origin of y-axis) and lateral-most position (origin of x-axis) of the
603 dendritic region.

604

605 **Figure 2 -** Locating functional input sites to DBNi1-2. Ai-iii) Representative example of the mid-point
606 of the $Ca^{2+}$ response to Ai) touch receptor stimulation, Aii) strain receptor stimulation and Aiii) visual
607 stimulation, each based on 30-40 repeats per stimulus, recorded in one animal. The ΔF/F (%) values
608 were binned over 2.5 pixels in x and y, and over 2.5 frames in time. Plots next to each image show the
609 fluorescence profile along the medio-lateral (M-L) axis (top) and the antero-posterior (A-P) axis (right);
610 values are normalised to the pixel with highest fluorescence change. Grey regions indicate pixel values
611 over the 75 % threshold, used for calculating the mid-point of the fluorescence response (see
612 Materials & Methods). The mid-point is indicated with black lines in plots, and grey lines in central

images. Axes next to images Ai-Aiv scale distance along the antero-posterior (A-P) dimension (left) and the medio-lateral (M-L) dimension (bottom). The origin of the axes is defined by the posterior-most point and the lateral-most point of the finger-like dendrites; posterior is to the bottom and lateral to the left of the images. Aiv) Combined imaging responses for all touch, strain and visual stimulation tests, colour code for sensory modalities indicated in top right.

Bi-iv) Mid-points of fluorescence responses to Bi) touch stimulation, Bii) strain receptor activation and Biii) visual stimulation. Biv) Overlay of all the mid-points in response to each modality of stimulation. N indicated in Figure. Note the complete overlap of two data points for strain.

C) A schematic, simplified representation of sensory input regions as indicated by $Ca^{2+}$ increases based on Aiv and Biv is overlaid with the maximum projection of a confocal stack from DBNi1-2 as revealed by staining with Alexa 568, data from same animal. Scale bar: 100 µm.

Di) Fluorescence responses over time obtained from three different ROIs, i.e. finger-like dendrites (fr), anterior region (ar) and junction region (jr) corresponding to the sensory input sites. Dii-Div Responses to touch (cyan), strain receptor activation (magenta), and visual stimulation (yellow) are shown for each ROI, respectively. Stimulus onset indicated by vertical grey line, averages of 5-8 presentations per stimulus. All recordings from one animal, different to animal in A.

E) Quantification of imaging responses. Ei) Peak fluorescence response shown as ΔF/F (%) for each ROIs (fr, ar and jr) for touch stimulation (cyan), strain receptor activation (magenta), and visual stimulation (yellow). Eii) Peak responses for each sensory modality normalised to the ROI showing the highest response. N = 4 preparations.

**Figure 3 –** Topographic organisation of $Ca^{2+}$ increases for flagellar touch receptors. A) Stimulating electrodes were inserted at three positions along the flagellum. Bi) Imaging the finger-like dendrites. Outline of the brain showing the region of mechanosensory afferent input (blue oval) and the area

637 imaged (grey square). Bii) Mean of 50 frames of *in vivo* $Ca^{2+}$ signal. The finger-like dendritic arborisation
638 is outlined by a thick dashed line. ROIs covering the anterior (a), middle (m) and posterior (p) dendrites
639 are indicated by thin dashed lines. C) Binned fluorescence increase (ΔF/F, %) in one animal upon
640 stimulation at Ci) 8 mm (5 repeats); Cii) 19 mm (5 repeats); and Ciii) 28 mm (3 repeats) from the base
641 of the flagellum. Binned over 5 pixels in x and y, and 2.5 frames in time. D) Overlay of pixels with mean
642 peak ΔF/F > 50 % of the maximum response, with stimulation at 8 mm (light blue), 19 mm (blue) and
643 28 mm (dark blue) along the flagellum; data binned over 10 pixel in x and y, and 5 frames in time. E)
644 Time-course of fluorescence responses (ΔF/F, %) in the ROIs 'a', 'm', and 'p' upon stimulation (stim)
645 at 8 mm (top), 19 mm (middle) and 28 mm (bottom) from the base of the flagellum. ROIs as indicated
646 in Bii. Fi) Mid-points of fluorescence responses upon electrical stimulation at different points along
647 the flagellum. The distance of stimulation sites to the base is indicated by shades of blue, scale given
648 underneath. Fii) Correlation between the positions of electrical stimulation along the flagellum as
649 measured from the base and the position of mid-point of fluorescence along the antero-posterior (A-
650 P) spread of the dendrites. G) Schematic diagram of topographic map as indicated by localised $Ca^{2+}$
651 signals. Afferents from the flagellum project to the brain with their proximal-to-distal position
652 represented along the posterior-to-anterior axis of the neuropile. Shades of blue represent
653 corresponding topography. Position of flagellar neuropile in the brain is indicated by a black box in
654 inset diagram of brain.

655

656 **Figure 4 –** Relationship between $Ca^{2+}$ signals and spiking response. A-C) $Ca^{2+}$ signal (ΔF/F, %) in ROIs
657 'fr', 'jr' and 'ar' are aligned with intracellular recording from a single branch of the finger-like dendrite.
658 ROIs (stippled lines) and recording site (black circle) indicated in the image at bottom centre. Data
659 from same animal, $Ca^{2+}$ signal and electrophysiology recorded subsequently as microelectrode was
660 removed to use high-power objective. Ai) Responses of 'fr' to touch receptor stimulation; Bi) response
661 to strain receptor stimulation; and Ci) response to visual stimulation. Stimulation times (stim)

662 indicated, with grey line and black bar below. Aii) Spike response to touch receptor stimulation at
663 higher temporal resolution. Three traces are shown for three positions of electrical stimulation along
664 the flagellum, as indicated on left. A plot of latency to first spike against distance along the flagellum
665 is given in the inset. Bii) Intracellular recorded response to strain at higher temporal resolution and
666 Cii) response to visual stimulation, respectively. D) Quantification of the intracellular response with
667 spikes per stimulus. E) Quantification of imaging response ΔF/F (%) per spike (N=4) for each ROI 'fr',
668 'jr' and 'ar' and for each mode of stimulation: touch (cyan), strain (magenta), and visual stimulation
669 (yellow).

670

671 **Figure 5 –** Effect of $Cd^{2+}$ on spikes generated by DBNi1-2. A) Action potentials recorded intracellularly
672 before and after application of $Cd^{2+}$, mean ± SD of 5 spikes at each time pre and post application. The
673 time constant (τ) of the repolarisation phase was measured for all spikes. B) Mean values of τ for 20
674 spikes before and 20 mins after bath application of $Cd^{2+}$ are indicated by grey circles (labelled time,
675 left axis); data from 3 different preparations. Relative value of τ normalised to response before
676 application of $Cd^{2+}$ is represented by black diamonds and pooled over three experiments, (labelled
677 normalised, right axis).

678

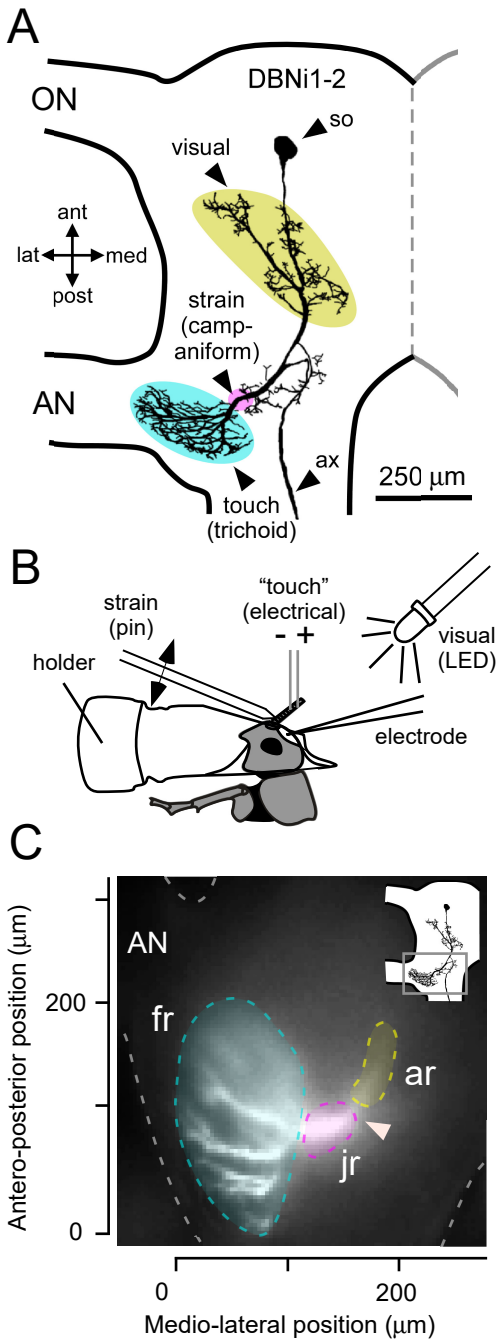
A
DBNi1-2
ON
so
visual
ant
lat
med
post
strain
(camp-
aniform)
AN
ax
250 µm
touch
(trichoid)
B
strain
(pin)
"touch"
(electrical)
- +
visual
(LED)
holder
electrode
C
AN
fr
ar
jr
200
0
Antero-posterior position (µm)
0
200
Medio-lateral position (µm)

Figure 1

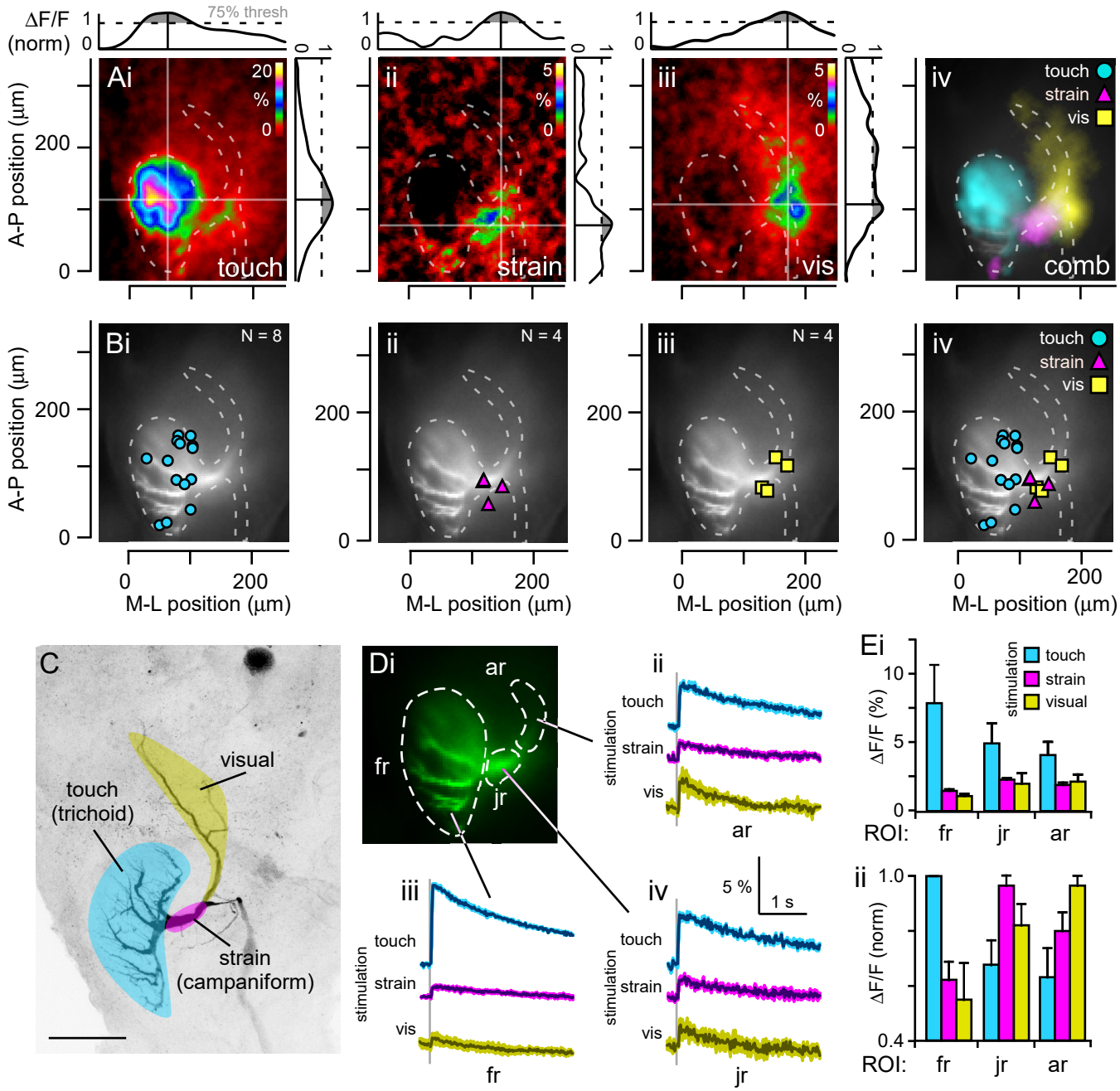
ΔF/F (norm)
75% thresh
Ai
ii
iii
iv
touch
strain
vis
comb
20 %
5 %
0
A-P position (μm)
200
Bi
N = 8
N = 4
M-L position (μm)
C
visual
touch (trichoid)
strain (campaniform)
Di
ar
fr
jr
stimulation
5 %
1 s
Ei
ΔF/F (%)
10
5
ROI:
fr
jr
ar
ΔF/F (norm)
1.0
0.4

Figure 2

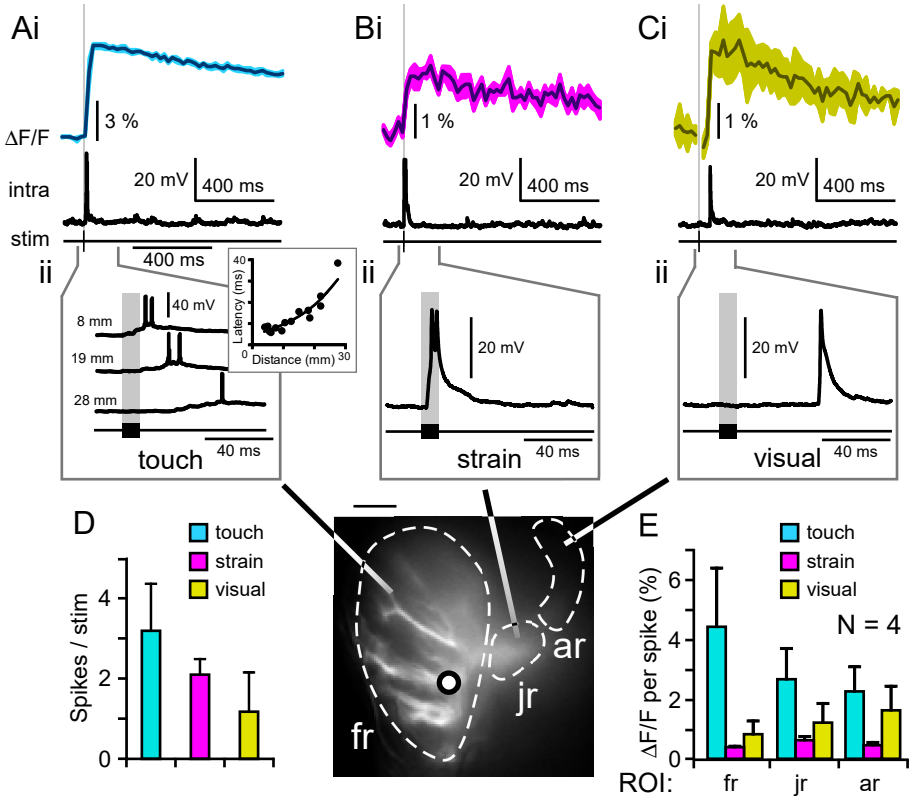
Ai
Bi
Ci
ΔF/F
3 %
1 %
1 %
intra
20 mV
400 ms
stim
ii
400 ms
40 mV
8 mm
19 mm
28 mm
touch
40 ms
Latency (ms)
Distance (mm)
strain
visual
D
Spikes / stim
touch
strain
visual
fr
jr
ar
E
ΔF/F per spike (%)
N = 4
ROI:

Figure 4

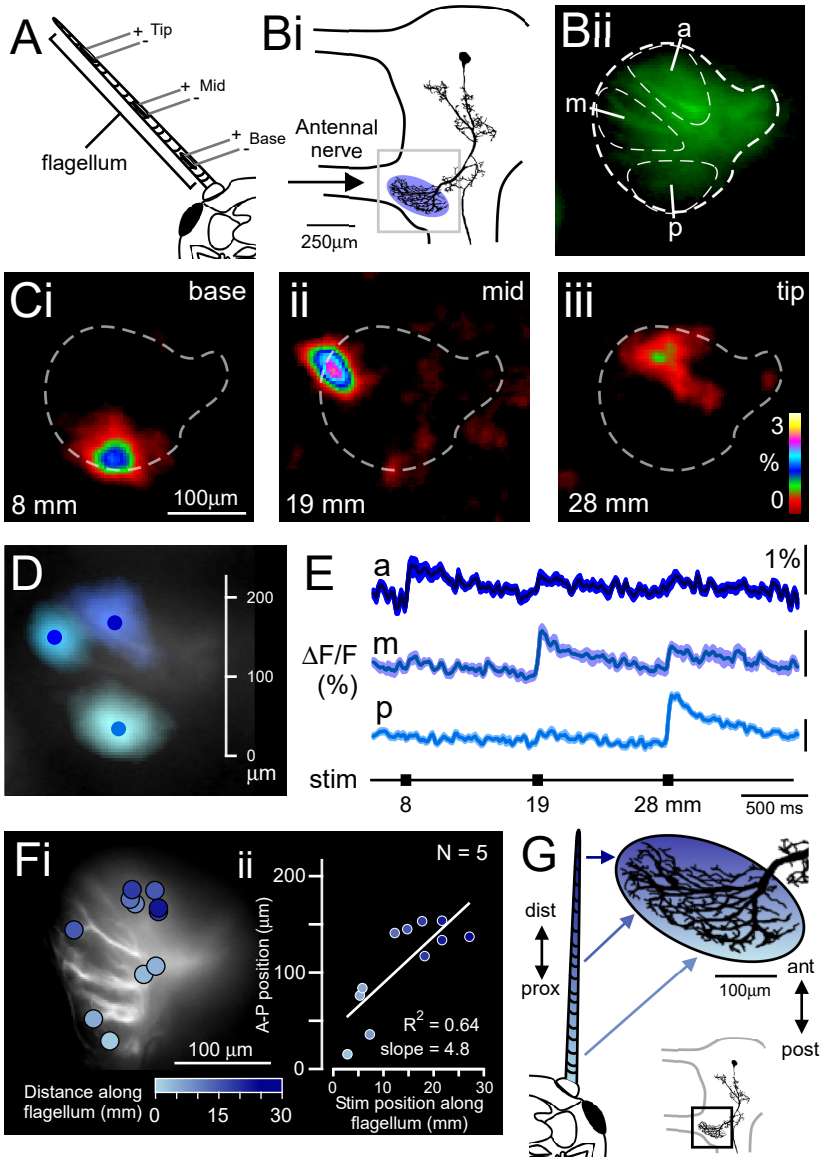
A
+ Tip
-
+ Mid
-
+ Base
-
flagellum
Bi
Antennal nerve
250µm
Bii
a
m
p
Ci
base
8 mm
100µm
ii
mid
19 mm
iii
tip
3
%
0
28 mm
D
200
100
0
µm
E
a
1%
ΔF/F (%)
m
p
stim
8
19
28 mm
500 ms
Fi
ii
N = 5
200
100
0
A-P position (µm)
100 µm
R2 = 0.64
slope = 4.8
0
10
20
30
Stim position along flagellum (mm)
Distance along flagellum (mm)
0
15
30
G
dist
prox
100µm
ant
post

Figure 3

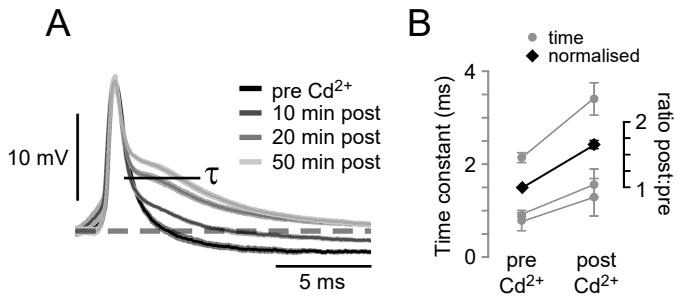
A
B
10 mV
τ
pre Cd2+
10 min post
20 min post
50 min post
5 ms
time
normalised
Time constant (ms)
4
2
0
2
1
ratio post:pre
pre
Cd2+
post
Cd2+

Figure 5